Simulating NMR relaxation with stochastic methods

Magnus Ögren

School of Science and Technology

Örebro University, Sweden

In collaboration with:

NanoGeoScience group at the University of Copenhagen

[1] M. Ögren, Eur. Phys. J. B (2014) 87: 255.
[2] M. Ögren, D. Jha, *et. al*., manuscript in preparation (2015).

Nuclear Magnetic Resonance

NMR important tool in modern technology.

Mobile Ex Situ High Resolution NMR

APPLICATIONS:

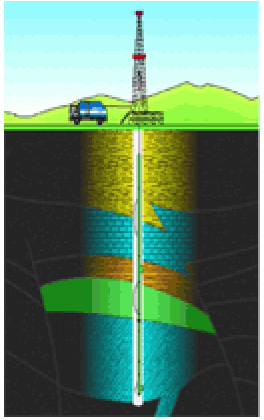
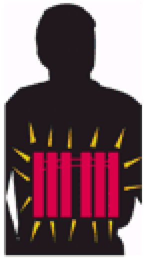


- Industrial sensing
- Oil well logging
- Medical imaging for large subjects
- Spectroscopy
- Imaging subjects or objects with ferromagnetic components
- Cargo inspection
- Stand-off detection

NMR important tool in modern technology.

Example of NMR log data from the North Sea

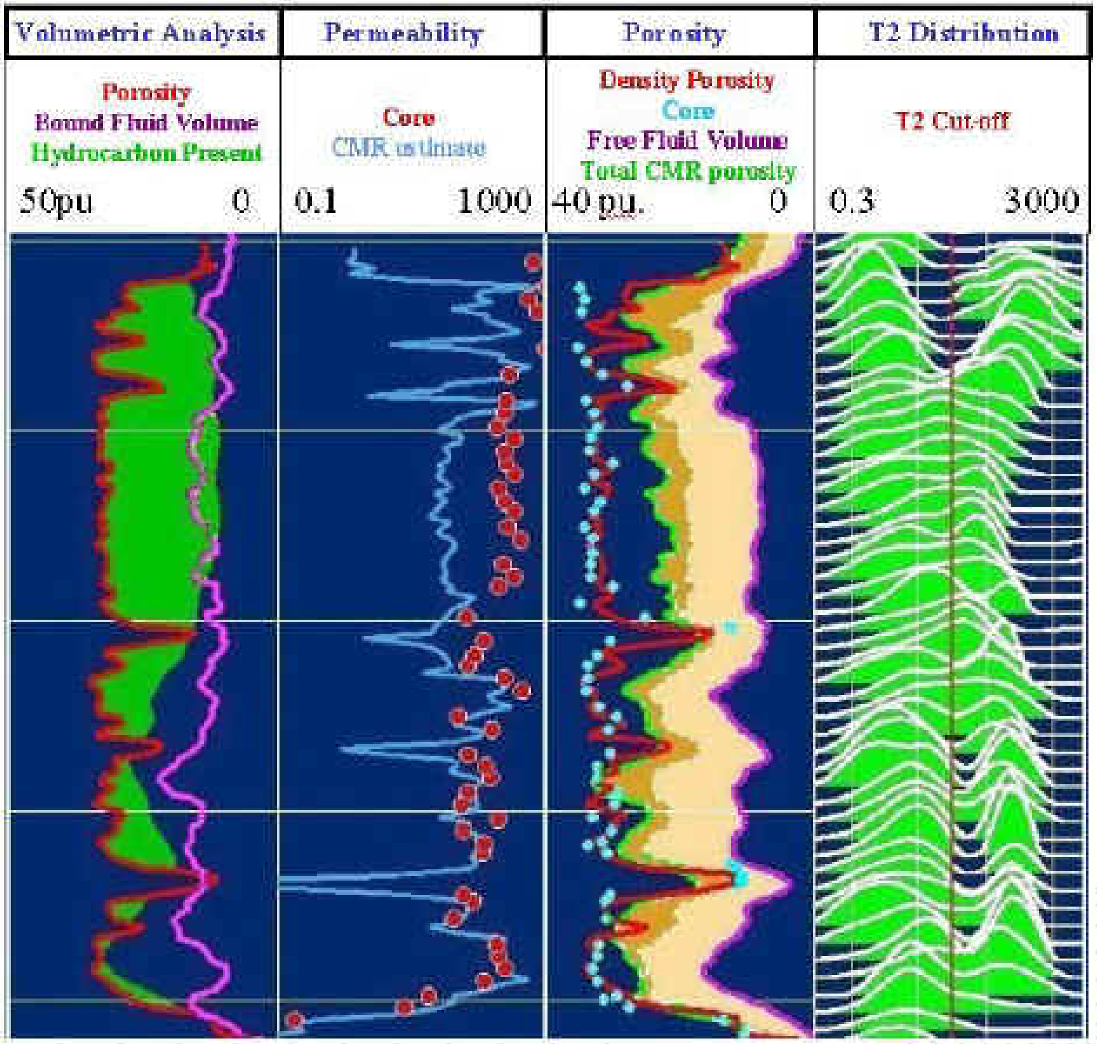

We see an increased use of 3D digital images of materials with complex structures within various applications.

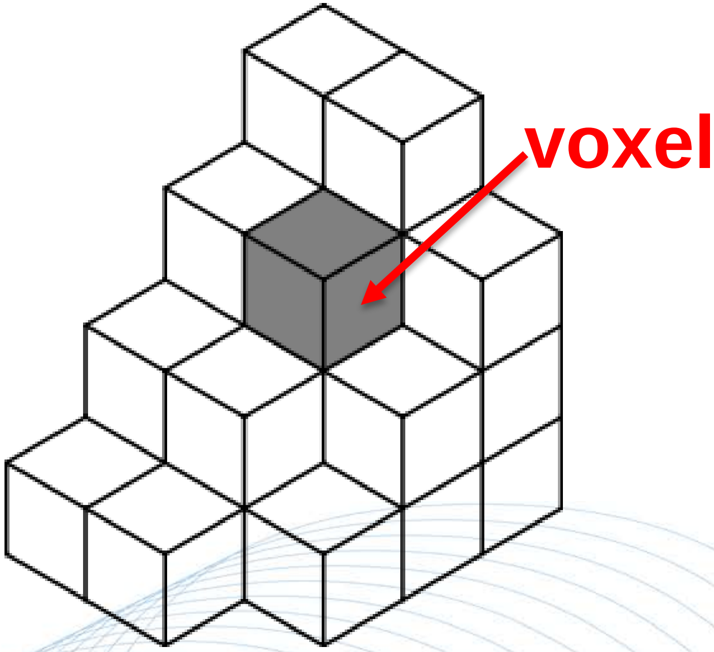

Input for manufacturing (reverse engineering)

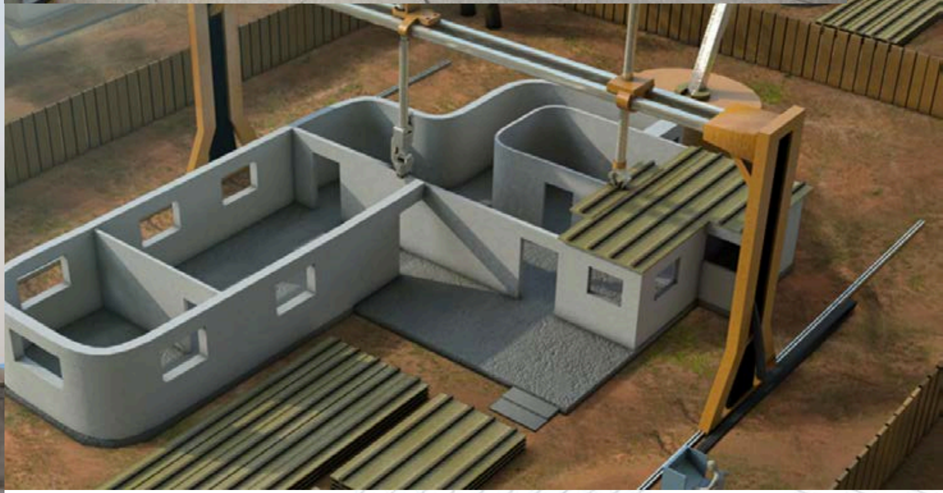

Output for measurements and quality control

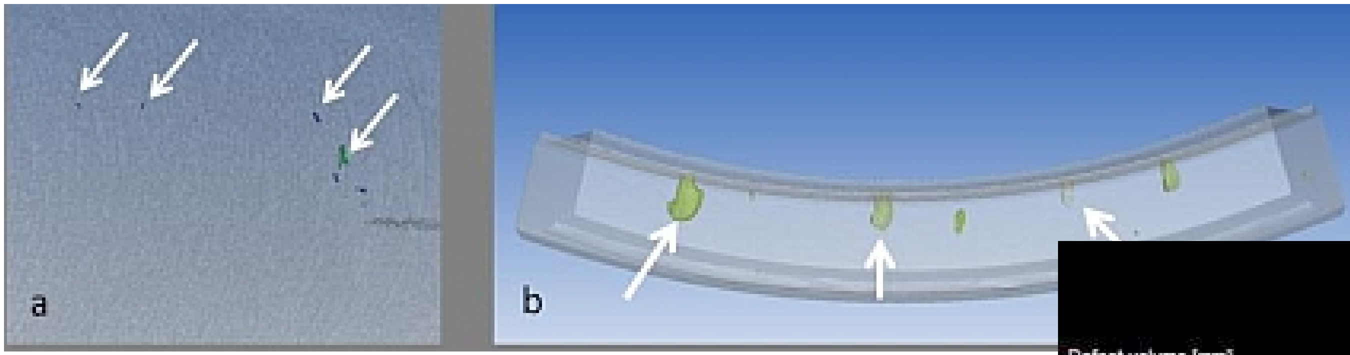

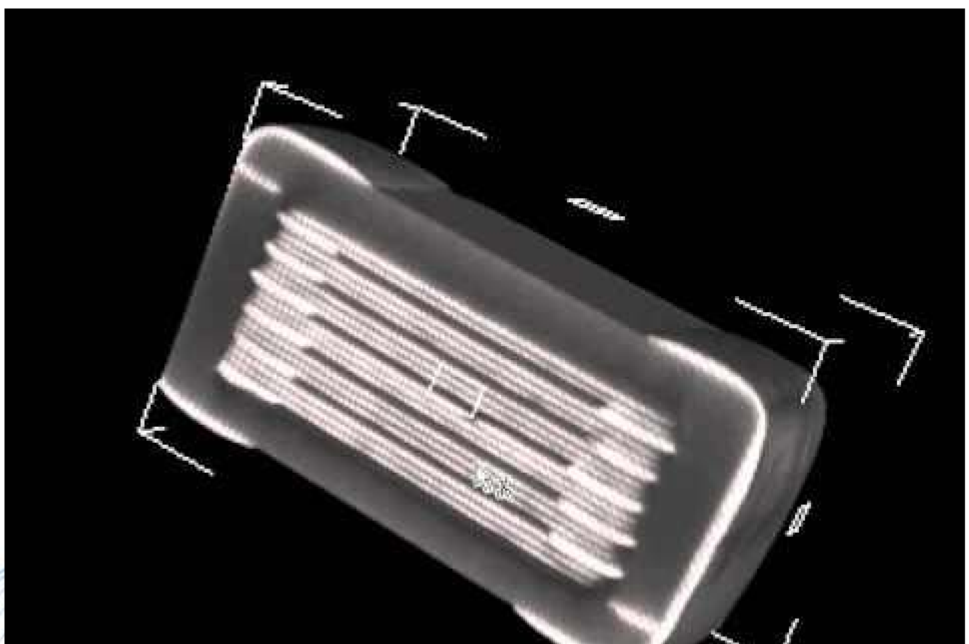

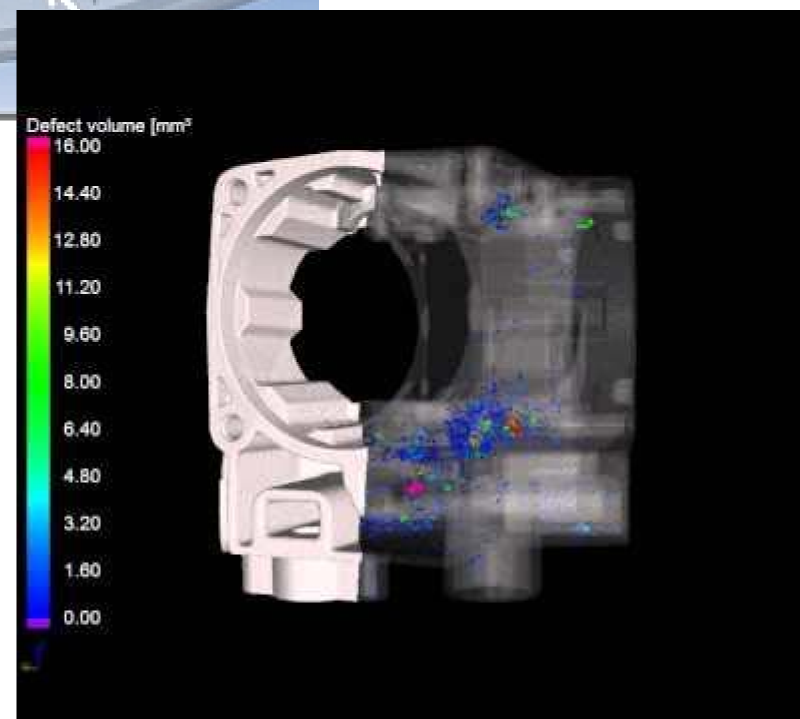

Present application: Understand some properties of large rocks from small samples…

↔

We use data from synchrotron radiation facilities.

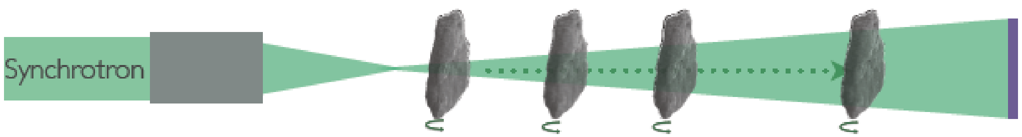

Measurement done at different positions in the conical beamline gives different resolution.

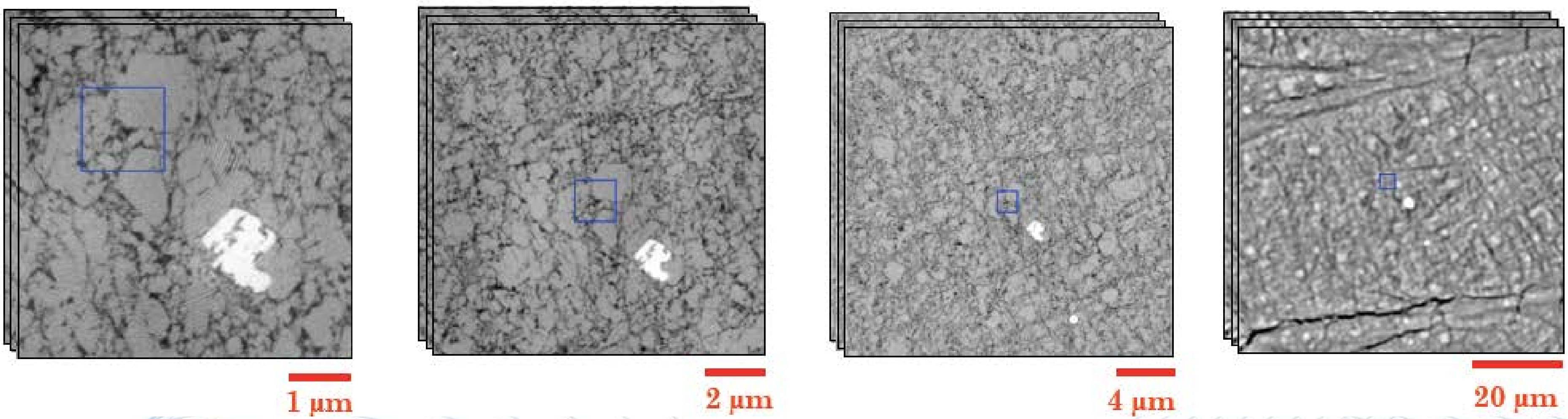

After simplifications of Bloch's equations

for NMR dynamics, we are left with a

reaction-diffusion equation

$$\frac{\partial M}{\partial t} = D_0 \nabla^2 M - \frac{M}{T_V},$$

with Robin boundary conditions

$$D_0 \mathbf{n} \cdot \nabla M + \rho M = 0.$$

We integrate out the spatial degrees

$$\mathcal{M}(t) = \int_\Omega M(\mathbf{x}, t)\, d\mathbf{x}$$

to obtain a time-dependent *total magnetization*

For uniform initial conditions, Gauss' theorem can provide the short time asymptote

$$\frac{1}{\mathcal{M}(0)} \left. \frac{d\mathcal{M}(t)}{dt} \right|_{t=0} = -\frac{\rho_0 S}{V}$$

In many applications the domain can be problematic…

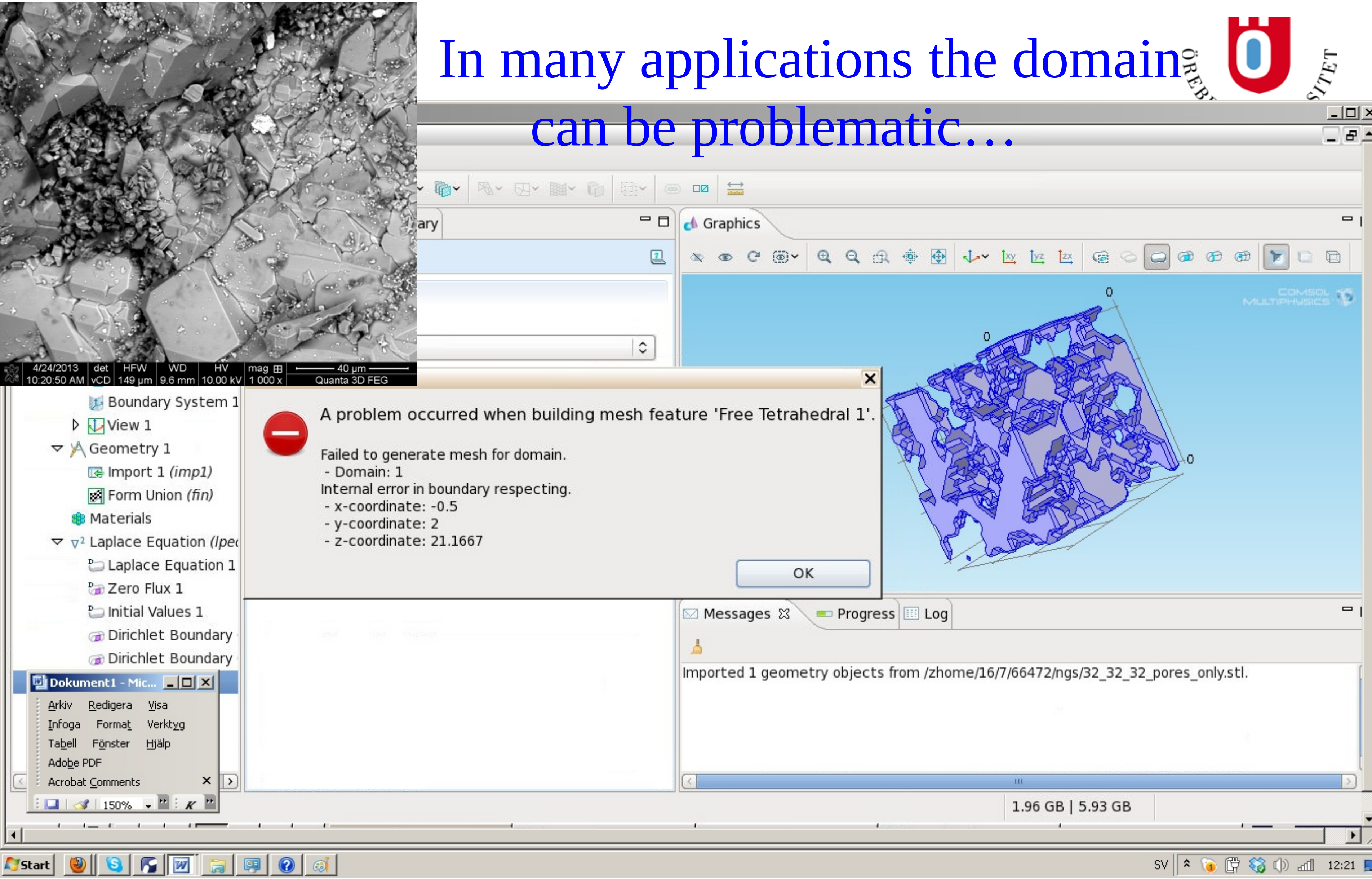

Try a random approach!

1.3.3. *Random walk method* (*RWM*). The RWM can be applied to find the local solution of *second-order* partial differential equations of the form

$$\frac{\partial u(\mathbf{x},t)}{\partial t} = \sum_{i=1}^{d} \alpha_i(\mathbf{x}) \frac{\partial u(\mathbf{x},t)}{\partial x_i} + \frac{1}{2} \sum_{i,j=1}^{d} \beta_{ij}(\mathbf{x}) \frac{\partial^2 u(\mathbf{x},t)}{\partial x_i \, \partial x_j} + q(\mathbf{x},t)\, u(\mathbf{x},t) + p(\mathbf{x},t) \tag{6}$$

where α_i, β_{ij} are real-valued functions defined on $\Re^d$, $d \geqslant 1$ is an integer, and q, p denote real–valued functions defined on $\Re^d \times [0,\infty)$. The domain of definition of Equation (6) is $D \times (0,\infty)$, where $D \subset \Re^d$ is an open bounded set. The solution $u: D \times (0,\infty) \rightarrow \Re$ depends on the initial and boundary conditions that need to be specified. The operator of Equation (6) includes a large number of interesting special cases; for example, parabolic, hyperbolic, elliptic partial differential equations in $\Re^2$ correspond to the steady–state version of Equation (6) with $d = 2$ and $\beta_{12}(\mathbf{x})\,\beta_{12}(\mathbf{x}) - \beta_{11}(\mathbf{x})\,\beta_{22}(\mathbf{x}) = 0$; >0; <0, respectively. Therefore, for example, the Laplace, Poisson and Helmholtz equations are special cases of Equation (6).

The RWM method can be applied to find the local solution of Equation (6) with Dirichlet and/or Neumann boundary conditions. The solution by this method involves three steps. *First*, a diffusion process $\mathbf{X}$ with generator coinciding with the differential operator of Equation (6) has to be constructed. *Second*, a relationship needs to be established between the value of the unknown function u at $(\mathbf{x},t) \in D \times (0,\infty)$, the boundary conditions, and an expectation depending on the sample paths of $\mathbf{X}$. Properties of diffusion processes, features of stochastic integrals, and Itô's formula can be used to obtain this relationship. *Third*, a Monte Carlo algorithm needs to be developed to estimate the expectation giving $u(\mathbf{x},t)$.

Laplace equation

Dirichlet BC at two opposite sides of the porous media (where the voltage or pressure difference is defined).

- Electric formation factor
- Pressure distribution (to be used for Stokes flows)

Poisson equation

Dirichlet BC, which means that the velocity is zero at the walls of pores.

- Local Stokes flow

Combine with pressure distribution to give flow through a porous media!

Diffusion equation

A mixed "Robin" BC.

- NMR-dynamics
- Surface reactions (crystal growth)

When discussing the convergence of a stochastic calculation we need to mention:

1) A large enough number of trajectories to obtain a statistically significant result;

2) A small enough step-size to explore the small scale geometry of the media. The latter issue is also directly connected to the resolution chosen for a digital media.

If conditions 1) and 2) are fulfilled, one can accuratelly simulate diffusion processes with Dirichlet ($\rho_0 \to \infty$) and Neumann ($\rho_0 \to 0$) boundary conditions in Eq. (4). However, for Robin boundary conditions we need to consider also a third point.

3) Probability based modeling of the surface relaxation, including:

3a) a correct (algorithm dependent) relation between the local probability for surface relaxation (p_a) and the function $\rho_0\,(\mathbf{x}, t)$;

3b) A local description of the surface area for a digital media.

3a) We have derived (first order) relation between parameters in PDE model and the RWM:

$$p_S = \Delta r \rho / D_0.$$

3b) We have constructed (first order) local boundary conditions that can be calculated "on the fly":

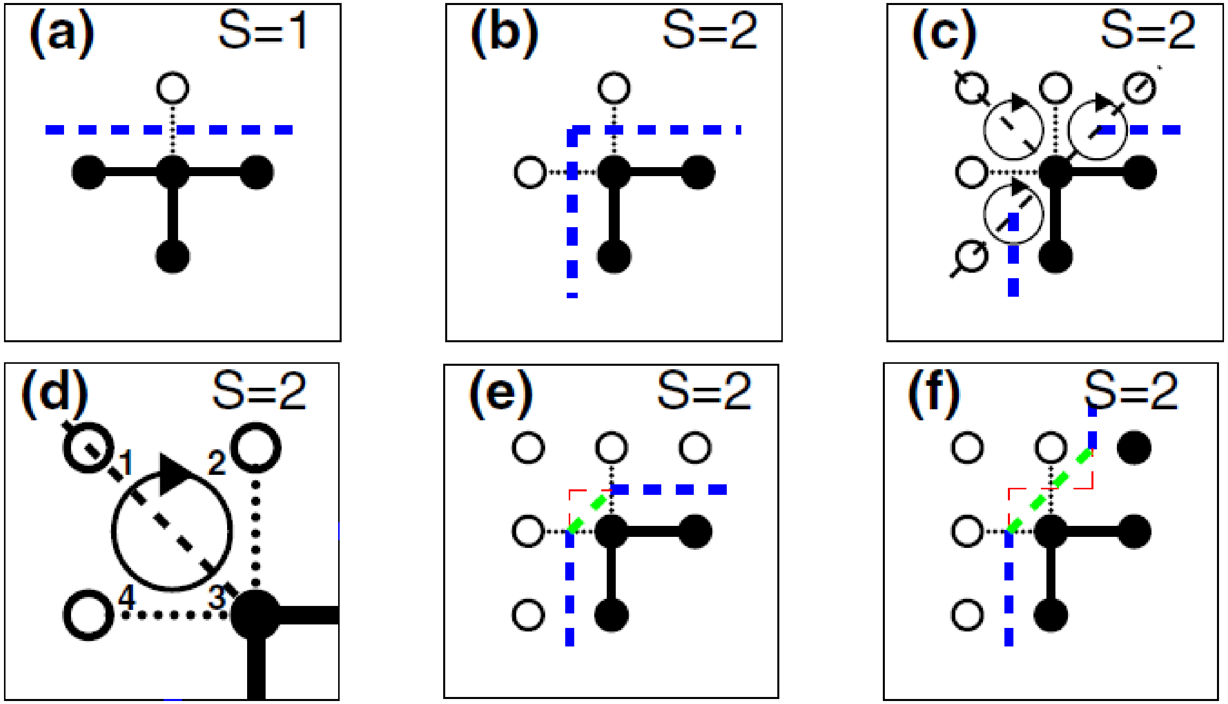

Above illustrated in 2D, generalized to any dimension.

In 2D the effects of ‘digitalization’ is easy to illustrate and quantify:

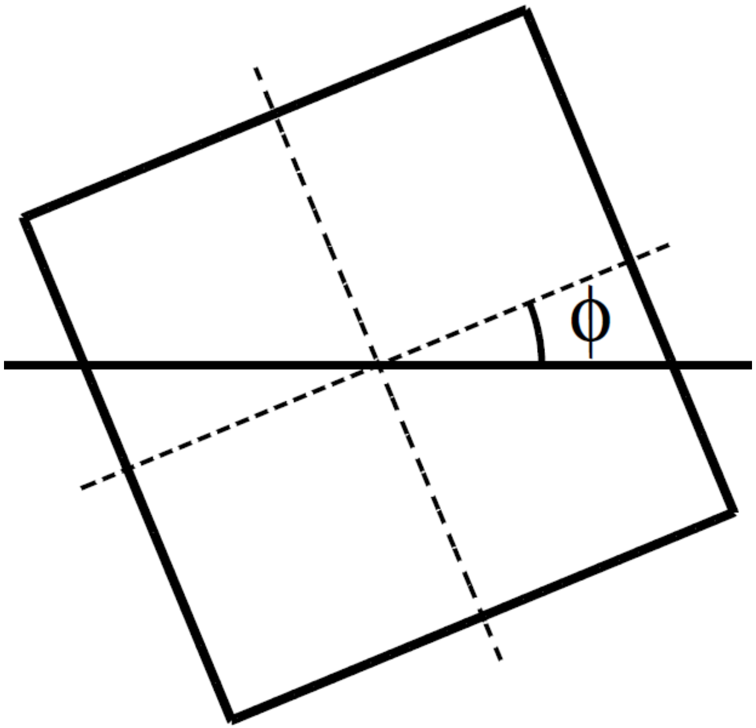

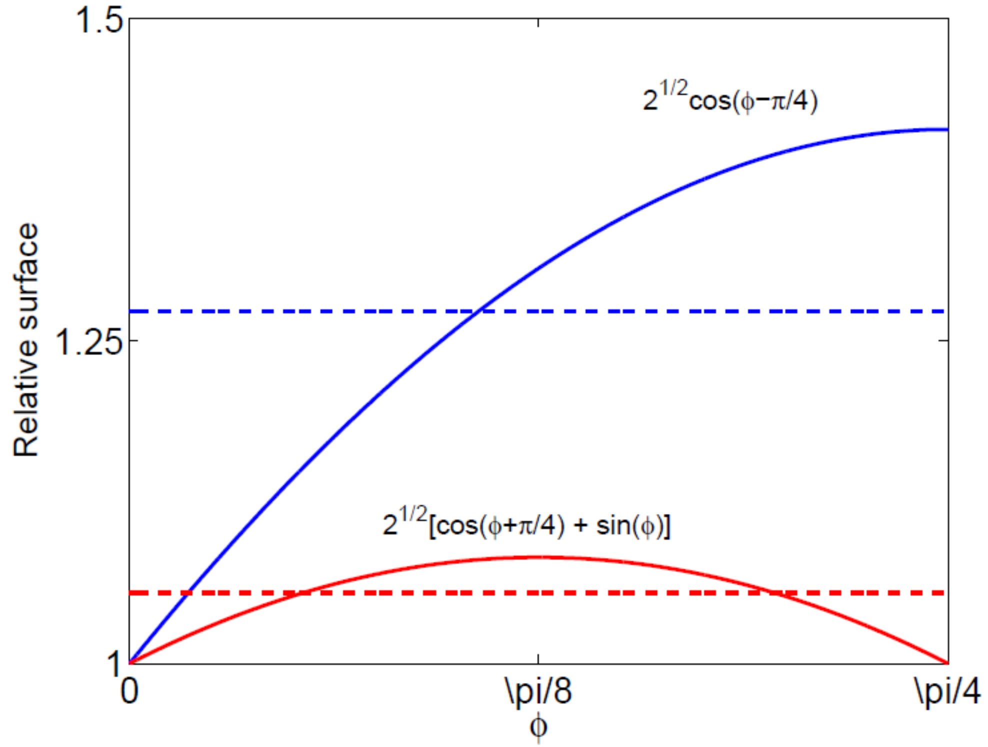

Comparative FEM simulations in 2D.

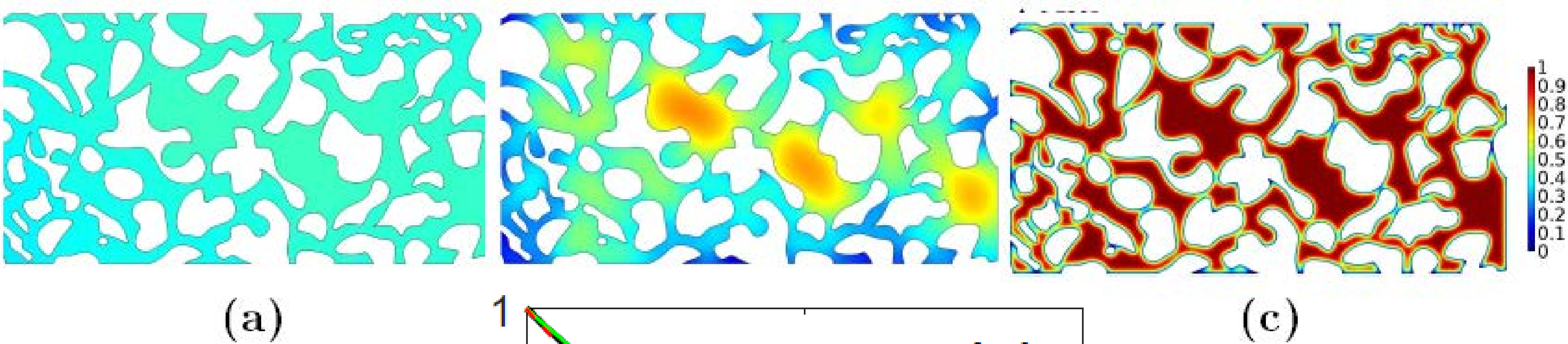

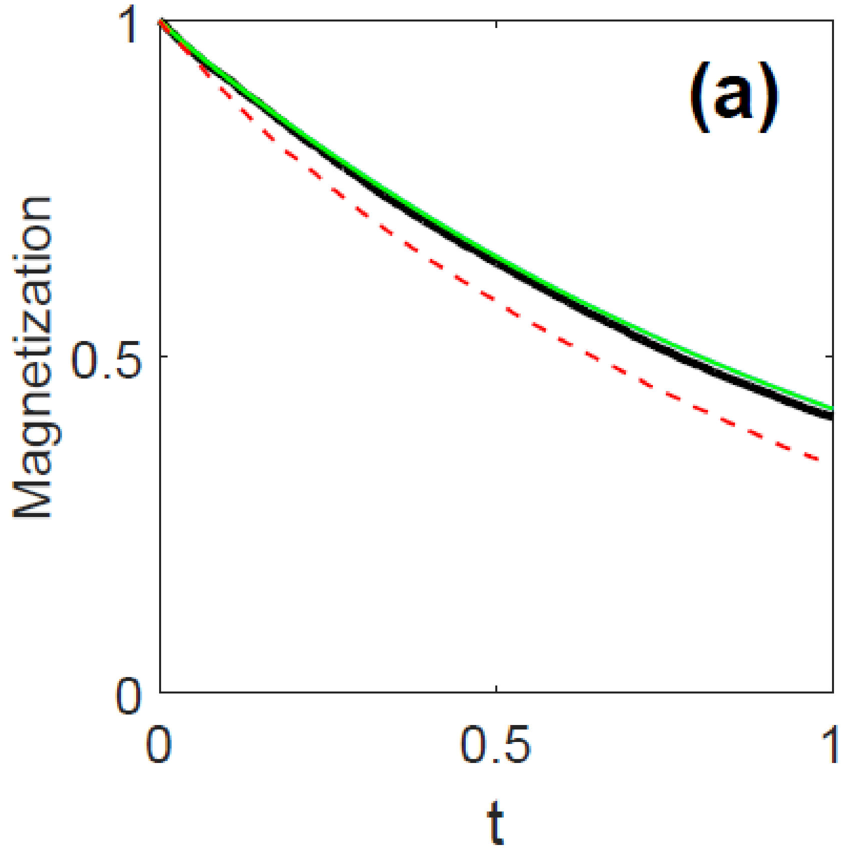

Comparison with analytic formulae: *Ball*

$$\mathcal{M}(t) = \mathcal{M}(0)\, 12 \sum_{j=1}^{\infty} \frac{\left[\sin\left(\sqrt{\lambda_j}\right) - \sqrt{\lambda_j}\cos\left(\sqrt{\lambda_j}\right)\right]^2}{\lambda_j^{3/2}\left[2\sqrt{\lambda_j} - \sin\left(2\sqrt{\lambda_j}\right)\right]} \exp\left(-\frac{D_0}{R_0^2}\lambda_j t\right), \quad (8)$$

where the eigenvalues λ_j are solutions of the equation $1 - \sqrt{\lambda_j}\cot\left(\sqrt{\lambda_j}\right) = R_0\rho/D_0$.

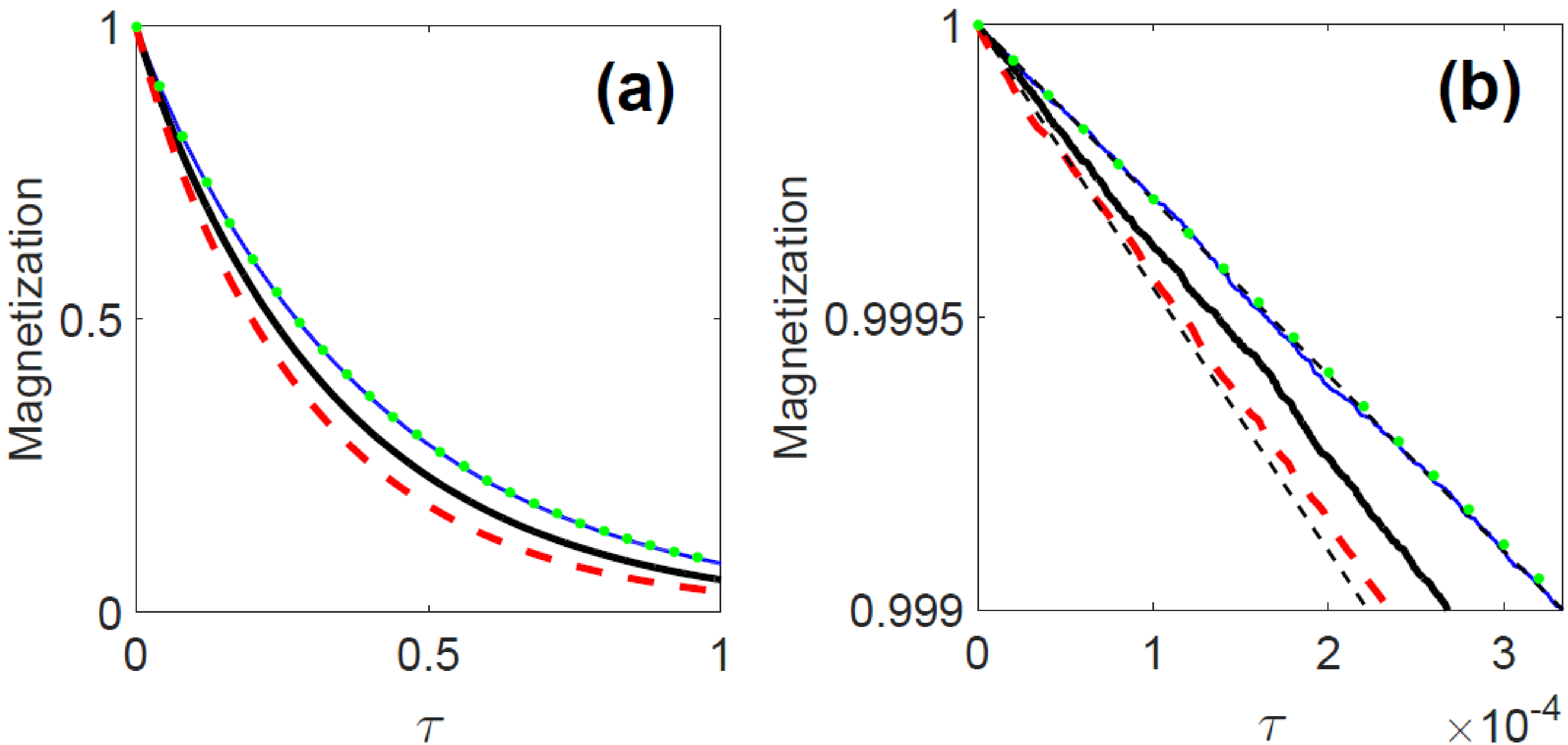

Comparison with analytic formulae: *Cube*

$$\mathcal{M}(t) = \mathcal{M}(0)\, 8 \left[\sum_{j=1}^{\infty} \frac{\sin^2\left(\sqrt{\lambda_j}\right)}{\sqrt{\lambda_j}\sin\left(\sqrt{\lambda_j}\right)\cos\left(\sqrt{\lambda_j}\right) + \lambda_j} \exp\left(-\frac{D_0}{R_0^2}\lambda_j t\right) \right]^3, \quad (9)$$

where the eigenvalues λ_j are solutions of the equation $\sqrt{\lambda_j}\tan\left(\sqrt{\lambda_j}\right) = R_0\rho/D_0$.

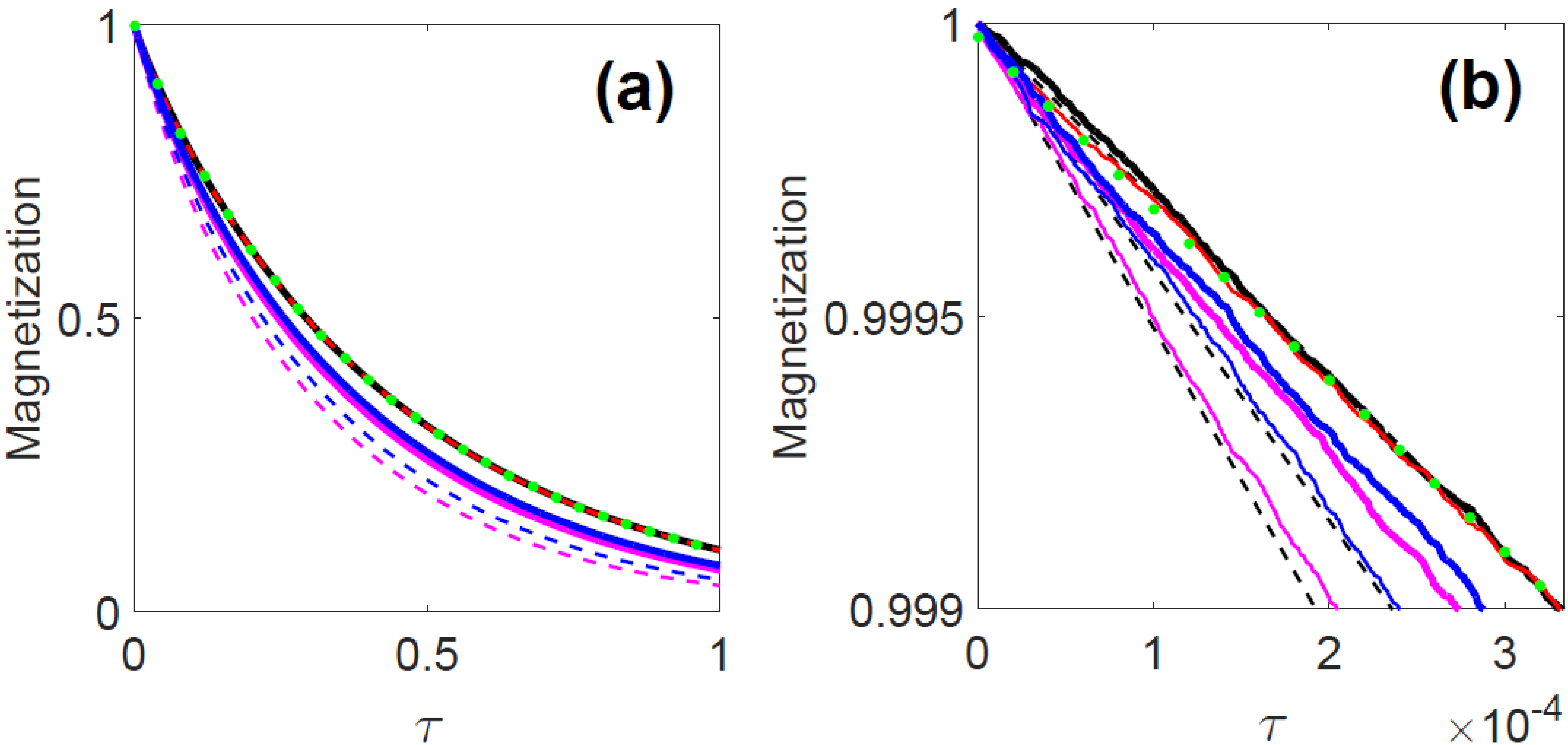

Present application…???

Simulations on 3D tomography images of chalk with a size in the order of $10^3 \times 10^3 \times 10^3$ voxels and resolution 10 nm

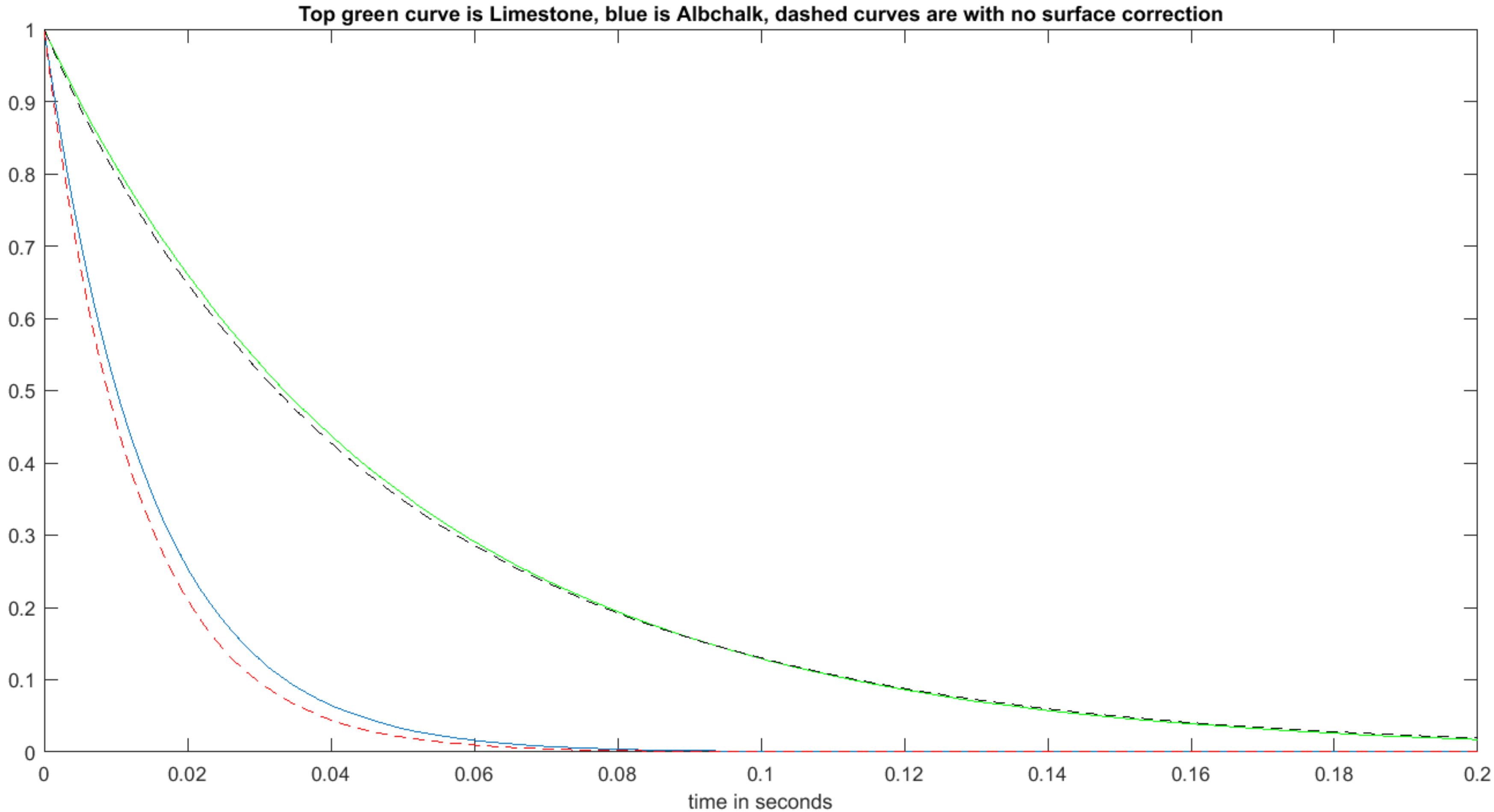

Spectral analysis, yet to be done!

Summary:

- **We can now perform stochastic simulations of PDE models defined on 3D digital images (>10^3*10^3*10^3) on standard computers with a ‘relevant’ accuracy.**

Outlook:

- **Optimize RWM algorithms and evaluate statistic accuracy for few trajectories (important “in field”).**
- **Develop a “Bismut” formula to directly calculate gradients (important for “flow”).**
- **Enter the area of strength of materials (important for “local collaborations”)**

Special thanks to PhD-student Diwaker Jha at the University of Copenhagen for providing data!

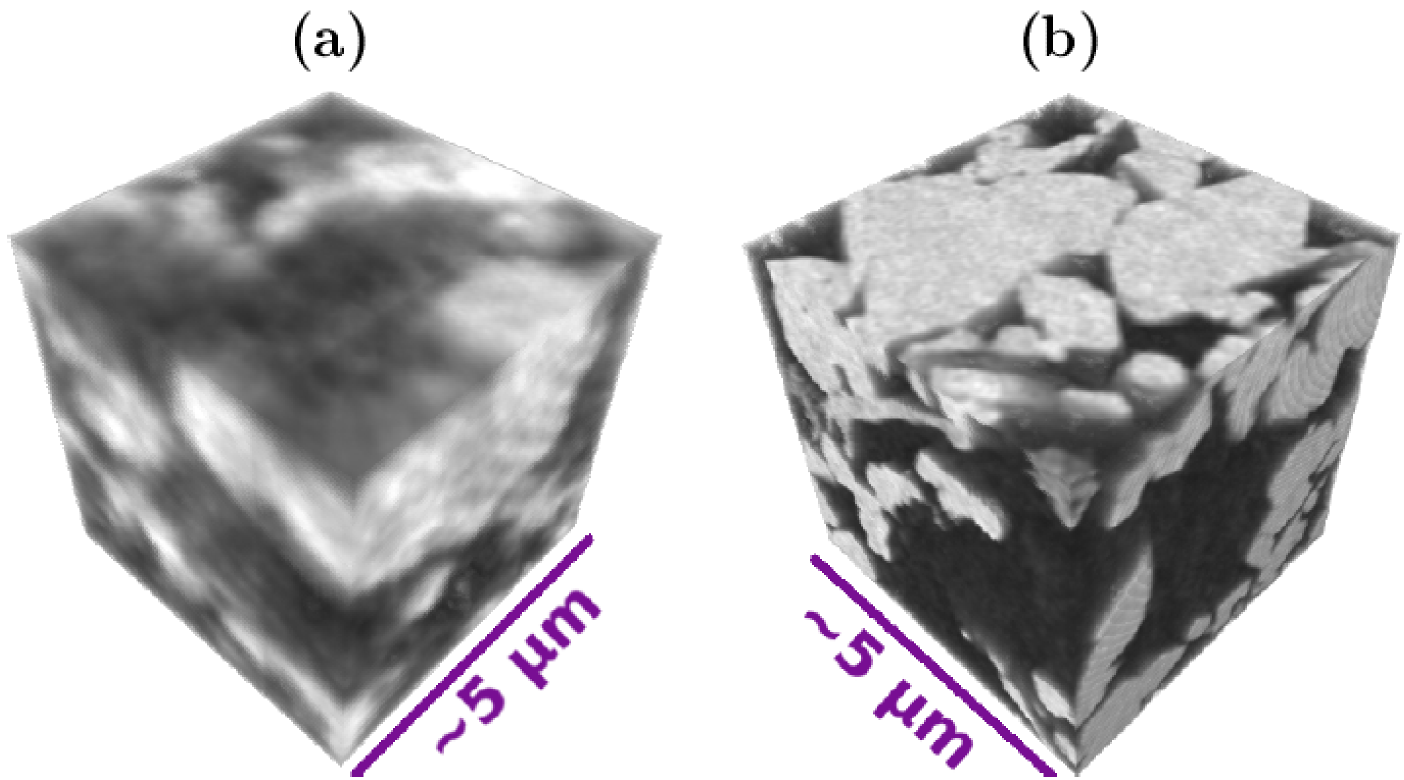

Figure 5: Examples of zooming in on regions in the CT-images for the two 3D chalk samples. To the left limestone (a) and to the right Aalborg chalk (b). Black ($Z = 1$) voxels constitutes the pore domain (assumed to be filled with brine). White ($Z = 0$) voxels represents regions of homogenous chalk. Aalborg chalk (b) contains a more complex pore morphology and was imaged with the new ptychography method, which explains the sharper image compared to (a). Since the sidelength of the full samples are in the order of $N\Delta r \simeq 25$ µm (see Table 2), the subvolumes shown here represents about 1% of the chalk sample domains in our calculations.